# Characteristics of the IR laser photothermally induced phase change in microchannels with different depths

Rong Chen[a,b]*, Xuefeng He[a,b], Xun Zhu[a,b]**, Qiang Liao[a,b], Liang An[c],
Zhibin Wang[a,b], Shuzhe Li[a,b]

[a] Key Laboratory of Low-grade Energy Utilization Technologies and Systems (Chongqing University), Ministry of Education, Chongqing 400030, China

[b] Institute of Engineering Thermophysics, Chongqing University, Chongqing 400030, China

[c] Department of Mechanical Engineering, The Hong Kong Polytechnic University, Hung Hom, Kowloon, Hong Kong, China

*Corresponding author. Tel.: 0086-23-65102474; fax: 0086-23-65102474; e-mail: rchen@cqu.edu.cn

**Co-corresponding author. Tel.: 0086-23-65102474; fax: 0086-23-65102474; e-mail: zhuxun@cqu.edu.cn

## Abstract

The photothermal effect induced phase change is an important phenomenon in optofluidics. In this work, therefore, the characteristics of the phase change in microchannels with different depths induced by a 1550-nm infrared laser under both low and high laser powers was visually studied. It was revealed that at low laser power, the liquid body could be always advanced as a result of the induced evaporation-condensation-coalescence process regardless the microchannel depth, which can be functioned as a micro pump. The μ-PIV testing results further demonstrated the coalescence was dominant mechanism in the interface advancement. Interestingly, although large depth increased the absorption length of the laser and thus improved the temperature and enhanced the evaporation, the advancing effect became weak due to the increase of both the flow resistance and liquid water content to be driven. At high laser power, for small depth microchannel, the liquid body was advanced at the beginning. Once a liquid slug along with a sealed gas slug was formed, the liquid body started to move backward, which can be functioned as chemical separation. However, as the microchannel depth increased, despite the evaporation was enhanced, such phenomena were hardly to happen because enhanced evaporation allowed large droplets to be generated. Air bubbles instead of gas slug were easily entrapped in the liquid body during the coalescence process. These air bubbles quickly grew up due to high temperature, which could obstacle the advancing movement of liquid body or even block the laser heating. Therefore, it can be concluded that the microchannel depth plays an important role in the photothermally induced phase change process. The obtained results are helpful for the design and operation of the photothermal effect based optofluidic micro-devices.

***Keywords:*** Optofluidics; photothermal effect; microchannel depth; phase change; absorption length

## 1 Introduction

Recently, the integration of microfluidics and optics has led to a new interdiscipline, i.e., optofluidics, which is a synergy of fluids, light and their interactions [1-6]. In optofluidic systems, the basic concept is to utilize the interactions between fluid and light to realize novel functions and applications [7-12]. Among these interactions, the photothermal effect is one of the most widely-used light induced physical effects, by which the light energy can be efficiently converted into heat. In particular, since the light can be easily focused to a tiny spot even with nano scale, the photothermal effect based optofluidic devices can realize rapid and precise non-contact manipulation of fluid flow and local temperature [13-15].

In the photothermal effect based optolfuidic devices, one of interesting phenomena is the photothermally induced phase change. Because the fluid in microchannels is confined in small space, in case the phase change occurs, there always exist consequent interfacial behaviors, such as the interface deformation, displacement, oscillation, reconstruction and so on [16-19]. Just because of these interfacial behaviors, specific applications can then be realized by the use of the photothermal effect. For instance, Liu et al. [20] used photothermal nanoparticles to allow a focused laser to become a local heating source. Through the photothermally induced evaporation-condensation-coalescence process, the liquid in the microchannel could be driven to move forward, which was functioned as a micropump. Zhang et al. [21] employed chromium pads embedded in microchannels as the photothermal conversion media. Once the laser was projected on the pads, microbubbles were generated by the photothermally induced phase change, which blocked the fluid flow to function as microvalves. Boyd et al. [22] developed an in-channel chemical separation method based on the photothermal effect induced phase change. In their work, an air bubble was used to segment the solution column into two parts. When the laser heated one end of the bubble, the intra mass transfer between the two ends of the bubble by the evaporation and condensation enabled the function of the chemical separation. However, in these optofluidic devices, the photothermal conversion materials are usually required to efficiently convert the light energy into the heat. Such design and operation make the chip more complex.

It should be noted that water is a typical solvent in biomedical applications, which can efficiently and directly absorb the infrared (IR) light. Hence, the direct absorption of light energy without the addition of the photothermal conversion materials is a promising way to develop the photothermal effect based optofluidic systems. In our previous studies [23], the IR laser photothermally induced condensation and meniscus evaporation were studied. One should note when the direct absorption of the laser energy is adopted, the depth of the microchannel becomes a crucial design parameter as it determines the absorption length of the laser. Subsequently, the photothermal efficiency is greatly affected, which in turn influences the phase change behaviors. Unfortunately, how the microchannel depth affects the photothermal effect induced phase change behaviors remains unclear. Therefore, it is necessary to attain better comprehension of the IR laser induced phase change process. To this end, the visual study was carried out to shed light on the IR laser photothermally induced phase change behaviors in this work. The emphasis was paid to the effect of the microchannel depth on the two-phase flow patterns under different laser powers and spot positions. The micro-particle image visualization (μ-PIV) was utilized to visualize the flow field in the liquid phase.

## 2 Experimental

In this study, all microchannels were fabricated by the SU-8 (SU-8 photoresist, Gersteltec Sarl, Switzerland ) lithography and PDMS ( Polydimethysiloxane, SYLGARD 184, Dow Corning, USA ) molding process. As illustrated in Fig. 1a, the microchannel was formed by assembling three PDMS layers. On the top layer, two holes were drilled as the inlet and outlet, respectively. The microchannel was fabricated in the middle layer with two built-in liquid tanks on both the ends of the microchannel to function as the liquid reservoir and pressure buffer unit. These two tanks faced the inlet and outlet, respectively. The bottom layer was used to seal the microchannel and the liquid tanks. These three PDMS layers were assembled before they were completely solidified, and then heated at 95 $^{o}$C for 20 minutes to enhance the bonding. Since the laser absorption length mainly depends on the microchannel depth, all tested microchannels were designed with the same width but different depths, which could be achieved by controlling the spin-coating speed and the total amount of the SU-8 photoresist. In this experiment, all fabricated microchannels shared the width of 200 μm, and the depth ranged from 100 μm, 200 μm, to 300 μm. The detailed information on the manufacturing parameters of the lithography and spin-coating processes are summarized in Table 1. The image of the fabricated microchannel is shown in Fig. 1b.

The visualized experimental system is illustrated in Fig. 2. As mentioned above, to reduce the complexity, an IR laser with the wavelength of 1550 nm and distilled water were chosen as the heating source and working fluid, respectively. The IR laser was focused by a coupled long working distance objective lens (NIR 10X objective, W.D. 30.5 mm, N.A. 0.26, Mitutoyo, Japan) with the spot diameter of 30 μm. The microchannel was fixed on the platform of a 3-aixs micro motion stage (LUGE, M150RX100Y100Z100-3, China) with step precision of 1 μm. An adjustable zoom lens (Navitar, Zoom 6000, USA) and a CMOS camera (Point Gray, Grashoper3, Canada) were used to acquire the real-time images in the microchannel. To ensure the coaxiality, the CMOS camera with the zoom lens was also fixed on a manually-controlled 3-axis translation stage. During the experiments, distilled water was slowly introduced into the microchannel through a high-precision syringe pump (Syringe Pump Model 33, Havard, USA) with PTFE tube connected to the inlet of the microchannel. The distilled water firstly fulfilled the liquid tank and then flowed into the microchannel. When the gas-liquid interface reached the experimental position, the pump was turned off. The laser was then focused to the desired location through the middle of the microchannel. The spot position was controlled by moving the microchannel sample located on the 3-aixs micro motion stage. To acquire the temperature variation in the microchannel without the disturbance to the phase change behaviors, an ex-situ temperature measurement was performed by inserting a micro thermocouple into the microchannel with the joint near the gas-liquid interface. During the ex-situ temperature measurement, only the temperature was measured without recording the phase change behaviors. In addition, the flow field during the laser heating was measured by a μ-PIV system (FlowMater, LaVison, Germany). Polymer microspheres (0.86 μm, Fluoro-Max, Thermo Scientific, USA) were added into the distilled water as fluorescent tracers. All experiments were repeated for 3 times.

## 3 Results and discussion

In our previous study [23], it was found that at low laser powers, the photothermal effect of the IR laser mainly induced the evaporation-condensation-coalescence process and thus caused the interface advancement of the original liquid body, while at high laser powers, the formation of the liquid slug in front of the interface of the original liquid body due to the coalescence between the condensed droplets caused the original interface to move backward. Such distinct behaviors arose from the changes of the evaporation rate and condensed droplet growth rate as well as the coalescence behaviors under different laser powers. In addition to the laser power, the variation in the microchannel depth can also influence the evaporation rate because of the resulting change of the absorption length of the IR laser. Moreover, the variation in the microchannel depth can also lead to the change of the flow resistance and the growth of the condensed droplets. Toward these two distinct phase change phenomena, therefore, the effects of the microchannel depth under low and high laser powers of 10 mW and 40 mW were studied in this work, respectively.

## 3.1 Low laser power

### *3.1.1 Dynamic behaviors*

In this sector, the dynamic behaviors of the IR laser induced phase change in a microchannel with the width of 200 μm and the depth of 100 μm were visually studied. The laser power was kept at 10 mW with the laser spot fixed at the location of 100 μm away from the initial interface of the liquid body. During the experiment, the location of the laser spot was unchanged. Fig. 3 shows the captured images of the photothermal effect induced phase change behaviors in the microchannel varying with the heating time.

It was observed that before the IR laser was illuminated to the liquid body, a convex meniscus in the front of the liquid body was formed due to the hydrophobic nature of the PDMS material. Once the IR laser was projected to the liquid body, the light energy was absorbed by liquid water and then immediately converted into the heat owing to the photothermal effect. The heat was transported to the interface to increase the temperature of the liquid water, leading to the evaporation from the interface. Since the IR laser was a typical local heating source, only the liquid water near the laser spot and the interface showed an increase in the temperature. In this case, the temperature of the surrounding air close to the interface remained at room condition (25 $^{o}$C, RH 60%). As a result, evaporated water vapor was easily condensed to form numerous tiny droplets in front of the liquid body, as shown in the image at the moment of 0.5 s. As the IR laser heating went on, more liquid water was evaporated to allow the growth of condensed droplets. As seen, the droplet sizes at the moment of 10 s were much larger than those at the moment of 0.5 s. On the other hand, with the growth of the condensed droplets, some neighboring droplets were coalesced with each other to form large droplets, which also made the droplet size larger. More importantly, some condensed droplets near the interface were coalesced with the original liquid body. The coalescence between the original liquid body and droplets could form a concave meniscus with large curvature, which lowered the local liquid pressure at the coalescing region of the interface [24]. Meanwhile, the coalescence caused the surface energy of the condensed droplets to be converted into the kinetic energy. Consequently, the lowered local liquid pressure along with the supplied surface energy pulled the original liquid body forward. As seen, the original liquid body moved forward for about 105 μm in 10 s and 268 μm in 60 s. When the liquid body was heated for 60 s, because of the evaporation and condensation, the temperature in the air space was also increased. The supersaturation of the water vapor became lower. Therefore, evaporated water vapor mainly contributed to the growth of the condensed droplets formed in previous moments, and the quantity of the droplets became less, which can be evidenced by comparing the captured images at 10 s and 60 s. In the meantime, some vapor could be transported to the region far away from the interface so that the area of the droplet formation was also extended. With the assistance of the photothermal effect induced evaporation-condensation-coalescence, the original liquid could then be continuously pulled forward. In this experiment, the original liquid body moved forward for 454 μm in 120 s.

From the above results, it can be known that the coalescence between the liquid body and condensed droplets is the main mechanism leading to the advancement of the interface. To further elaborate the effect of the coalescence, the velocity change within the liquid body was visualized by μ-PIV. The results are presented in Fig. 4, which shows the case of the liquid body coalescing with a single droplet. As shown in Figs. 4a and 4b, during the droplet was merged with the liquid body, a concave meniscus was formed at the coalescence position to lower the liquid pressure, which was consistent with the above analysis. More importantly, from the velocity field shown in Fig. 4c, it can be seen that because of the coalescence, the liquid velocity near the coalescence region was immediately increased and the liquid water in other region tended to flow to the coalescence position. Hence, the interface of the original liquid body can be advanced. This fact further demonstrates that the coalescence between the liquid body and droplets is the main mechanism to pump the liquid water. Since the energy required for pumping the liquid water comes from the surface energy of the droplet, the size of the droplet plays an important role in this process. For this reason, the effect of the droplet size on the velocity change within the liquid body was also investigated. Note that the droplet size cannot be precisely controlled in this process. The droplets with different sizes were selected from the observations. Meanwhile, because the coalescence mainly affected the liquid velocities in the coalescence region, we chose the largest liquid velocity during the coalescence process as the representative velocity to reflect the effect of the droplet size on the coalescence. The results are shown in Fig. 5. As seen, when the liquid body coalesced with large droplets, the induced liquid velocity increased. This is mainly because more surface energy with large droplet can be converted into the kinetic energy during the coalescence process, leading to an increase in the liquid velocity. As a result, the larger droplet, the higher liquid velocity. In addition to the coalescence between the liquid body with a single droplet, the coalescence between the liquid body and multiple droplets also frequently occurred. Therefore, the velocity change caused by the coalescence with multiple droplets was visualized. The results are shown in Fig. 6. Unlike the coalescence with a single droplet where only velocities in a small region close to the coalescence position increased, much larger region exhibited the increment of the liquid velocity because of increased coalescing area. Moreover, the maximum liquid velocity of $1.2\times10^{-4}$ m/s, which was much larger than those of the cases of the coalescences with a single droplet, was observed. This is because the simultaneous coalescence between the liquid body and multiple droplets led to more surface energy to be released. Consequently, the liquid velocity was greatly improved. In addition, because the coalescence area was enlarged, the liquid water in other region flowed to these places instead of a small coalescence region, making the velocity distribution more uniform. In summary, the above visualization results further reveal that the coalescence dominates the interface advancement.

### *3.1.2 Effect of the microchannel depth*

As mentioned earlier, the variation in the microchannel depth can cause the change of the absorption length and flow resistance, influencing the advancing effect of the coalescence. Based on the Beer-Lambert law, the laser power absorbed by water can be calculated by equation (1) [25],

$$\eta = 1 - e^{-\alpha d} \tag{1}$$

where $\eta$ is the absorptivity of the laser, $\alpha$ = 10.9 cm$^{-1}$ is the absorption coefficient of 1.55 μm in water, $d$ is the optical depth, i.e., the mirochannel depth. Clearly, the total absorbed energy is mainly determined by the microchannel depth. Therefore, the effect of the microchannel depth was studied. In this work, the microchannel width was maintained at 200 μm while the microchannel depth ranged from 100 μm, 200 μm to 300 μm and the corresponding laser absorptivity was 10.3% 19.6% and 27.9%, respectively. In the meantime, since the laser spot position influences the thermal resistance to the interface and the interface temperature and evaporation rate, the effect of the laser spot position was also investigated in this work. The laser spot position ranged from 100 μm to 500 μm away from the initial interface of the liquid body. Based on our visual results, it was found that at the low laser power of 10 mW, all cases showed the advancement of the interface due to the photothermally induced evaporation-condensation-coalescence. This fact indicates that the low laser power heating mainly causes the pumping mechanism. For this reason, the average interface moving speed can be utilized to access the effect of the microchannel depth. The average interface moving speed can be determined from the total interface moving distance over by the total laser heating time. Fig. 7 shows the variations of the average interface moving speed with the microchannel depth and laser spot position. It is seen that increasing the distance between the laser spot and initial interface led to the reduction in the average interface moving speed. It is easy to understand that the increase of the distance between the laser spot and initial interface resulted in an increase in the thermal resistance from the laser spot to the interface and thus lowered the interface temperature, which can be verified by the measured maximum liquid water temperature near the interface shown in Fig. 8. As seen, the maximum liquid water temperature decreased with increasing the distance between the laser spot and initial interface. Accordingly, the evaporation rate was decreased and the growth of the condensed droplets also became slow. Under such a circumstance, the photothermally induced evaporation-condensation-coalescence less took place. The advancing effect was weakened with large distance between the laser spot and initial interface so that the average interface moving speed was lowered. More interestingly, regardless the laser spot position, the increase of the microchannel depth led to the decrease of the average interface moving speed. This trend was opposite to the variation of the measured temperature with the microchannel depth. As shown in Fig. 8, large microchannel depth exhibited a high maximum liquid water temperature. Such temperature response to the microchannel depth can be attributed to the increase of the absorption length. In this case, more light energy can be absorbed and be converted into the heat, thereby increasing the temperature. At the same time, however, the increase of the microchannel depth increased the liquid-solid interface area. In this context, the viscous drag was also increased to resist the liquid flow. On the other hand, increasing the microchannel depth indicated more liquid water entered into the microchannel. It is meant that the photothermally induced evaporation-condensation-coalescence process had to pull more liquid water forward, which also lowered the interface moving speed. As a result, although the increase of the microchannel depth could improve the evaporation rate, which benefited for the occurrence of the photothermally induced evaporation-condensation-coalescence, the resulting negative factors of the increased viscous drag and liquid water mass became predominant. Therefore, increasing the microchannel depth resulted in a slow interface moving speed in spite of high temperature.

In reality, the properties of the used liquids may be different. Hence, to generalize the results to other liquids, we introduced the Capillary number (*Ca*) to analyze the results,

$$Ca = \frac{\mu \cdot v}{g \cdot \sigma} \tag{2}$$

where $\mu$ and $\sigma$ are the viscosity and surface tension of distilled water corresponding to the measured maximum liquid water temperature shown in Fig. 8, $v$ is the average interface moving velocity and $g$ is the gravitational acceleration. The results under different microchannel depths at the laser power of 10 mW are shown in Fig. 9. As can be seen, the *Ca* was much smaller than 1, indicating the capillary force is dominant in this process. In addition, it can be seen that the variation of the *Ca* was similar to the change of the average interface moving speed. Therefore, it can be known that the interface advancement is predominated by the surface tension. The changes of the liquid and microchannel wettability can lead to the variation in the average interface moving speed.

## 3.2 High laser power

Different from the low laser power heating, it was found that the condensed droplets would coalesce with each other to form a liquid slug in front of the original liquid body because of high evaporation and condensation rates resulting from the high laser power heating in our previous study [23]. After the formation of the liquid slug, the original liquid body would move back instead of the interface advancing. Clearly, the variation of the microchannel depth can also cause the change of the evaporation rate. As a result, the effect of the microchannel depth at high laser power heating was also investigated in this work. Similarly, the microchannel width was kept at 200 μm while the microchannel depth changed from 100 μm, 200 μm to 300 μm. The laser power was fixed at 40 mW.

### *3.2.1 Small microchannel depth*

First of all, we studied the photothermal effect induced phase change behavior in the microchannel with small microchannel depth of 100 μm. The visualization results are shown Fig. 10. It can be seen that before the laser heating started, the supplied liquid water tended to form a convex meniscus in the front due to the hydrophobic nature of the PDMS. Once the IR laser was projected to the liquid water, the photothermal effect induced evaporation was immediately actuated. Clearly, because of the high laser power heating, more heat could be generated to enhance the evaporation from the interface. Similar to the case of the low laser power heating, since the IR laser was a tiny local heating source, the evaporated vapor was condensed to form lots of small droplets in front of the interface. These droplets coalesced with each other to form large droplets. Some droplets also coalesced with the interface of the original liquid body, lowering the local liquid pressure inside the original liquid body and releasing the surface energy. As such, the original liquid body was pulled forward. The original liquid body moved forward for 34 μm in 10 s and 323 μm in 60 s, Compared with low laser power heating of 10 mW, the advancement in the interface was smaller in 10 s but larger in 60 s. This is mainly because larger laser power causes higher evaporation rate and faster growth speed of droplets. Accordingly, more frequent coalescence between droplets happened to form bigger droplets. On the other hand, less coalescence between droplets and the liquid body took place such that the interface advancing became weak in the first 10 s. Although the advancement of the liquid body was weak with large laser power in the first 10 s, the sizes of condensed droplets near the interface were much bigger than those with low laser power. As the laser heating went on, these bigger droplets finally coalesced with the interface of the original liquid body, resulting in more remarkable advancements of the interface in 60 s. However, because the evaporation rate was higher with larger laser power, more vapor could be transported to the region far away from the interface to be condensed to the droplets. The area of the droplet formation was much extended, which can be evidenced by comparing the captured images at the same moments shown in Figs. 3 and 10. For this reason, the droplets formed in the region far away from the interface had more time to grow up. On the other hand, the coalescence between the condensed droplets also assisted the growth of these droplets in the faraway region. As a result, some large droplets were coalesced with each other to form a liquid slug in front of the original liquid body with a sealed air slug, as shown in the image captured at t=133 s in Fig. 10. After the liquid slug formation, the interface movement of the original liquid body changed, that is, the interface started to move backward instead of the advancing, as shown in the captured images at t=180 s and 240 s in Fig. 10. This behavior is due to the fact that the evaporated vapor tended to be condensed at the interface of the liquid slug to make it grow rather than the droplet formation. Under such a circumstance, the interface advancing caused by the coalescence between the original liquid body and condensed droplets became unavailable. The mass loss of the original liquid body could not be compensated by the coalescence, leading to the backward movement of the interface of the original liquid body. Such phase change process allows it to be functioned as chemical separation. These results were similar to the previously-reported results [23]. This fact also indicates that the coalescence between the original liquid body and droplets is the main driving force to realize the mechanism of pumping the original body.

### 3.2.2 *Large microchannel depth*

Fig. 11 shows the dynamic behaviors of the photothermal effect induced phase change in the microchannel with the depth of 200 μm. As seen, at the beginning, the IR laser heated up water and increased the interface temperature as a result of the photothermal effect. The increased interface temperature caused the liquid water to be evaporated from the interface and then the vapor condensed to form several droplets in front of the original liquid body. The droplets coalesced with the interface to lower the liquid pressure inside the original liquid body and release the surface energy. As such, the original liquid body was pulled forward. In the first 20 s, the interface could be advanced for 200 μm, which was lower than 306 μm for the microchannel with 100 μm in depth. This is definitely because increasing the microchannel depth led to an increase in the advancing resistance, which was similar to the circumstances of low laser power cases. In this case, more light energy was absorbed to generate the heat so as to increase the liquid water temperature due to higher laser power. As shown in Fig. 12, for all laser spot positions, the microchannel depth of 200 μm yielded larger temperature than did the microchannel depth of 100 μm. As mentioned earlier, the increased temperature enhanced the interface evaporation so that more water vapor could be generated to form more droplets in front of the interface. However, the growth of the microchannel depth increased the flow resistance and the total amount of liquid water to be driven, which reduced the evaporation-condensation-coalescence advancing mechanism. Therefore, though the evaporation rate and the growth rate of the droplet were greatly improved in this case, the increase of the microchannel depth finally resulted in a lower interface moving speed. Besides, unlike the case of the microchannel with 100 μm in depth, in which a liquid slug was formed, the formation of a liquid slug in the microchannel with 200 μm in depth was not observed. This is because large microchannel depth increased the difficulty in the liquid slug formation by the coalescence between the large droplets. Large microchannel depth broadened the cross-section area. In this case, the condensed droplets had to grow big enough along the depth direction to seal the channel.

Unfortunately, the increased depth made the formation of the liquid slug become unavailable. Although the liquid slug was not formed, the growth rate of the droplet was rather large as a result of high evaporation rate to form much large droplets, as shown in the image at t=158 s in Fig. 11. Under such a circumstance, when these large droplets coalesced with the interface of the original liquid body, air bubbles were easily entrapped in the moving liquid body as shown in the image at t=159 s in Fig. 11. Different from the above case with relatively small microchannel depth and large laser power and the previously reported results [23], where the entrapped bubbles were almost unchanged because of relatively low water temperature, the entrapped bubbles were gradually growing up in this measurement, as shown in the images at t=240 s and t=415 s of Fig. 11. This distinct behavior could be contributed to the high water temperature, which could enhance the evaporation so as to allow the air bubble to grow up. In this period, the photothermal effect induced evaporation-condensation-coalescence could still advance the original interface of the liquid body. However, the air bubble reduced the area of the liquid flow, increasing the flow resistance. Besides, the air had low thermal conductivity and the interface of the original liquid body became far away from the laser spot, increasing the thermal resistance and thus lowering the evaporation rate. Both of them slowed down the moving speed of the original liquid body. For example, in the first 158 s, the interface moved forward for 200 μm, while it only moved forward for 140 μm after the gas bubble formation from t=159 s to t=415 s. The average interface moving speeds were $1.3\times10^{-5}$ m/s and $0.05\times10^{-5}$ m/s, respectively. Moreover, at t=416 s, the air bubble could grow and coalesced with each other to form a gas bubble with the connection to both the side walls. Based on the observations, one may question that the coalescence was to form a gas slug instead of a large gas bubble with the connection to both the side walls. In fact, it can be concluded by analyzing the visual results. As seen, after 416 s, the formed gas bubble was almost unchanged except another small gas bubble growth was observed and some small droplets were formed at the wall inside of the air bubble. This phenomenon was caused by the equilibrium between the evaporation and condensation occurring in the gas bubble, leading to the unchanged gas bubble. More importantly, because the coalescence induced the formation of the large gas bubble instead of the gas slug, the original liquid body was not cut into two parts and the original liquid body was still continuous. The photothermally induced evaporation-condensation-coalescence could continue to take place in the front of the liquid body to advance the interface, which could be evidenced by the captured image at t=435 s. In addition, it can be known that if the gas slug was formed, the original liquid body would be cut into parts. A liquid slug would be formed in the front, which was similar to the case with small microchannel depth of 100 μm and large laser power. Under such a circumstance, as mentioned above, the evaporated water vapor mainly condensed at the interface of the liquid slug so that the coalescence between the interface and droplets was hardly to occur to drive the liquid body to move forward. Therefore, the interface of the gas slug facing to the laser spot should move backward in the case of the gas slug formation. However, in this case, such backward movement of the interface was not found in our observations, indicating that a large gas bubble with the connections to both side walls was formed instead of the gas slug formation.

To further prove this point, we shut down the IR laser and directly pumped the liquid water into the microchannel from the inlet. As shown in Fig. 13, the gas bubble was remained at its original location and the pumped water drove the original interface to move forward. It is easy to understand that if the gas slug was formed to cut the original liquid body into two parts, when the liquid water was pumped into the microchannel, the gas slug should be pushed and move forward. However, such phenomenon did not happen. This fact further proved that an air bubble was formed instead of a gas slug. Because of this, unlike small microchannel depth where a liquid slug was formed with a sealed gas slug, the liquid water could be continuously pulled forward in the microchannel with large depth in spite of the large air bubble formation.

In addition to the air bubble formation between the laser spot and original interface, another interesting phenomenon was also observed in the microchannel with large depth of 300 μm. As shown in Fig. 14, at the beginning, the photothermal effect induced evaporation-condensation-coalescence was able to advance the movement of the interface as a result of the lowered liquid pressure inside the original liquid body and the surface energy released from the droplets. Because large microchannel depth increased the absorption length, more light energy could be absorbed to be converted into the heat so as to increase the interface temperature. The growth rate of the droplet was quickly increased to form large droplets. When the interface coalesced with the relatively large droplets, air was easily trapped in the original liquid body. Different from the above case, some air could be trapped at the location near the laser spot to form small air bubbles, as shown in the image at t=23 s of Fig. 14. Due to the high water temperature resulting from large absorption length, liquid water was also evaporated from the interface of the air bubbles, making these air bubbles grow up. However, since the air bubbles was rather close to the laser spot, the ever-growing air bubbles could occupy the space of the laser spot, as shown in the images at t=60 s and t=90 s. Because the IR laser could be well absorbed by liquid water, the air bubbles yet located at the laser spot hindered the light energy absorption, leading to much less heat to be generated. The photothermal effect induced evaporation ceased. Therefore, although the IR laser was still projected to the microchannel, no phase change behavior was actuated. From these two cases, it is implied that although the increase of the microchannel depth can enhance the evaporation due to the increased absorption length, once the air bubbles are formed in this process, the phase change behavior is greatly affected and may become rather unstable. Careful selection of the microchannel depth is critically important to realize the photothermal effect based microfluidic devices.

## 4. Conclusions

In this work, the IR laser photothermally induced phase change of distilled water in the microchannels with different depths and laser powers were studied. Visualized experimental results indicated the two-phase flow pattern and the interfacial behaviors in microchannels were greatly affected by the laser power and the microchannel depth.

Under the low laser power of 10 mW, the liquid body could be driven to move forward through the evaporation-condensation-coalescence process in the microchannel with small depth. Through the μ-PIV testing results, it was revealed that the coalescing speed increased with increasing the condensed droplet size. The coalescence with multiple droplets led to higher advancing speed compared with the single droplet coalescence case. As the depth of microchannel increased, the increased absorption length of the IR laser led to higher temperature within the liquid body. Although the evaporation could be enhanced, the interface advancing speed became lower. This is mainly because larger depth increased the flow resistance and the total amount of liquid water to be driven, weakening effect of the evaporation-condensation-coalescence and thereby resulting in the lowered interface advancing speed. Under the high laser power of 40 mW, a liquid slug with a sealed air slug tended to be formed in the microchannel with small depth. The interface of the original liquid body started to move backward. The phase change behavior switched from the pumping effect to chemical separation effect. This is not the case for the microchannels with large depth. The formation of a liquid slug along with a sealed gas slug was not observed due to the increased microchannel depth, which increased the difficulty in the liquid slug formation due to the droplets coalescence. However, because the increased microchannel depth improved the absorption length of the IR laser, improving the temperature and enhancing the evaporation. The growth rate of droplets became rather high to form large droplets so that air bubbles were easily entrapped in the original liquid body during the coalescence process. Owing to the high temperature, the growth of the entrapped air bubbles could then obstacle the advancing of liquid body or even block the laser heating. Therefore, the design of the microchannel is critically important in operating the photothermal effect based optofluidics. The obtained results are also helpful for the optimization of the operating conditions in this type of microdevice.

## Acknowledgements

The authors gratefully acknowledge the financial supports of the National Natural Science Foundation of China (No. 51222603 and No.51276208), National Natural Science Funds for Distinguished Young Scholar (No.51325602) and the Program for New Century Excellent Talents in University (NCET-12-0591).

## References

1. Monat, C.; Domachuk, P.; Grillet, C.; Collins, M.; Eggleton, B. J.; Cronin-Golomb, M.; Mutzenich, S.; Mahmud, T.; Rosengarten, G.; Mitchell, A. Optofluidics: a Novel Generation of Reconfigurable and Adaptive Compact Architectures. *Microfluid Nanofluid* **2007**, *4* (1-2), 81.
2. Psaltis, D.; Quake, S. R.; Yang, C. Developing Optofluidic Technology Through the Fusion of Microfluidics and Optics. *Nature* **2006**, *442* (7101), 381.
3. Pang, L.; Chen, H. M.; Freeman, L. M.; Fainman, Y. Optofluidic Devices and Applications in Photonics, Sensing and Imaging. *Lab on a Chip* **2012**, *12* (19), 3543.

4. Oliva-Ramirez, M.; González-García, L.; Parra-Barranco, J.; Yubero, F.; Barranco, A.; González-Elipe, A. R. Liquids Analysis with Optofluidic Bragg Microcavities. *ACS Appl. Mater. Interfaces* **2013**, *5* (14), 6743.

5. Donner, J. S.; Baffou, G.; McCloskey, D.; Quidant, R. Plasmon-Assisted Optofluidics. *ACS Nano* **2011**, *5* (7), 5457.

6. Monat, C.; Domachuk, P.; Eggleton, B. J. Integrated Optofluidics: a New River of Light. *Nature Photonics* **2007**, *1* (2), 106.

7. Yuan, L.; Huang, J.; Lan, X.; Wang, H.; Jiang, L.; Xiao, H. All-in-Fiber Optofluidic Sensor Fabricated by Femtosecond Laser Assisted Chemical Etching. *Opt. Lett., OL* **2014**, *39* (8), 2358.

8. Sun, Y.; Shopova, S. I.; Frye-Mason, G.; Fan, X. Rapid Chemical-Vapor Sensing Using Optofluidic Ring Resonators. *Opt. Lett., OL* **2008**, *33* (8), 788.

9. Zhu, H.; White, I. M.; Suter, J. D.; Dale, P. S.; Fan, X. Analysis of Biomolecule Detection with Optofluidic Ring Resonator Sensors. *Opt. Express, OE* **2007**, *15* (15), 9139.

10. Levy, U.; Shamai, R. Tunable Optofluidic Devices. *Microfluid Nanofluid* **2008**, *4* (1-2), 97.

11. Zhu, H.; Mavandadi, S.; Coskun, A. F.; Yaglidere, O.; Ozcan, A. Optofluidic Fluorescent Imaging Cytometry on a Cell Phone. *Anal. Chem.* **2011**, *83* (17), 6641.

12. Venancio-Marques, A.; Barbaud, F.; Baigl, D. Microfluidic Mixing Triggered by an External LED Illumination. *J. Am. Chem. Soc.* **2013**, *135* (8), 3218.

13. Feng, X.; Gao, F.; Xu, C.; Gaoming, L.; Zheng, Y. Self Temperature Regulation of Photothermal Therapy by Laser-Shared Photoacoustic Feedback. *Opt. Lett., OL* **2015**, *40* (19), 4492.

14. Motosuke, M.; Shimakawa, J.; Akutsu, D.; Honami, S. Noncontact Manipulation of Microflow by Photothermal Control of Viscous Force. *International Journal of Heat and Fluid Flow* **2010**, *31* (6), 1005.

15. Maxim N Slyadnev; Yuki Tanaka; Manabu Tokeshi, A.; Takehiko Kitamori. Photothermal Temperature Control of a Chemical Reaction on a Microchip Using an Infrared Diode Laser. *Anal. Chem.* **2001**, *73* (16), 4037.

16. Yang, S.-C.; Fischer, W.-J.; Yang, T.-L. Size-Controllable Micro-Bubble Generation Using a Nanoimprinted Plasmonic Nanopillar Array Absorber in the Near-Infrared Region. *Appl. Phys. Lett.* **2016**, *108* (18), 183105.

17. Hu, W.; Ishii, K. S.; Fan, Q.; Ohta, A. T. Hydrogel Microrobots Actuated by Optically Generated Vapour Bubbles. *Lab on a Chip* **2012**, *12* (19), 3821.

18. Ming Pan; Minkyu Kim; Kuiper, S.; Tang, S. K. Y. Actuating Fluid-Fluid Interfaces for the Reconfiguration of Light. *IEEE J. Select. Topics Quantum Electron.* **2015**, *21* (4), 444.

19. Amy N Hellman; Kaustubh R Rau; Helen H Yoon; Stephanie Bae; James F Palmer; K Scott Phillips; Nancy L Allbritton, A.; Vasan Venugopalan. Laser-Induced Mixing in Microfluidic Channels. *Anal. Chem.* **2007**, *79* (12), 4484.

20. Liu, G. L.; Kim, J.; Lu, Y.; Lee, L. P. Optofluidic Control Using Photothermal Nanoparticles. *Nature Materials* **2005**, *5* (1), 27.

21. Zhang, K.; Jian, A.; Zhang, X.; Wang, Y.; Li, Z.; Tam, H.-Y. Laser-Induced Thermal Bubbles for Microfluidic Applications. *Lab on a Chip* **2011**, *11* (7), 1389.
22. Boyd, D. A.; Adleman, J. R.; Goodwin, D. G.; Psaltis, D. Chemical Separations by Bubble-Assisted Interphase Mass-Transfer. *Anal. Chem.* **2008**, *80* (7), 2452.
23. He, X.; Chen, R.; Liao, Q.; Wang, H.; Zhu, X.; Xu, Q.; Li, S.; Xiao, S. IR Laser Assisted Photothermal Condensation in a Microchannel. *Chemical Engineering Science* **2014**, *119*, 288.
24. Chen, R.; Li, S.; Wang, H.; Liao, Q.; Zhu, X.; Fan, Q.; He, X.; Wang, Z. Dynamic Behavior of the Liquid Flow Coalescing with a Droplet in Hydrophobic Microchannels. *Journal of Nanoscience and Nanotechnology* **2015**, *15* (4), 2923.
25. Xu, R.; Xin, H.; Li, Q.; Yang, X.; Chen, H.; Li, B. Photothermal Formation and Targeted Positioning of Bubbles by a Fiber Taper. *Appl. Phys. Lett.* **2012**, *101* (5), 054103.

## Table list

Table 1 Manufacturing parameters of SU-8 lithography and spin-coating

| channel depth (μm) | SU-8 weight (g) | spin speed (rpm) | spin-coating time (s) |
|---|---|---|---|
| 100 | 2.75 | 1200 | 50 |
| 200 | 3.16 | 1000 | 50 |
| 300 | 3.72 | 900 | 30 |

## Figure Captions

**Figure 1** (a) Illustration of the microchannel assembly and (b) the image of the fabricated microchannel.

**Figure 2** Schematic diagram of the visualized experimental system.

**Figure 3** Phase change behaviors in a 200 μm×100 μm microchannel (Laser power: 10 mW, spot position: 100 μm).

**Figure 4 (a)** Raw particle image before coalescence, **(b)** during coalescence, **(c)** Velocity vector map of liquid column during the coalescence with single droplet in a 200 μm×100 μm microchannel (Laser power: 10 mW, spot position: 100 μm).

**Figure 5** Effect of the coalesced droplet size on the average maximum coalescing speed in the liquid column (Laser power: 10 mW, spot position: 100 μm).

**Figure 6 (a)** Raw particle image before coalescence, **(b)** during coalescence, **(c)** Velocity vector map of liquid column before and during the coalescence with multiple droplets in a 200 μm×100 μm microchannel (Laser power: 10 mW, spot position: 100 μm).

**Figure 7** Effect of the microchannel depth on the average interface moving speed (Laser power: 10 mW).

**Figure 8** Variations in the maximum liquid water temperature with the microchannel depth and laser sport position (Laser power: 10 mW).

**Figure 9** Variation of Capillary number with the microchannel depth and laser spot position. (Laser power: 10 mW)

**Figure 10** Phase change behavior in a 200 μm×100 μm microchannel (Laser power: 40 mW, spot position: 100 μm).

**Figure 11** Phase change behavior in a 200 μm×200 μm microchannel (Laser power: 40 mW, spot position: 100 μm).

**Figure 12** Variations in the maximum liquid water temperature with the microchannel depth and laser spot position (Laser power: 40 mW).

**Figure 13** Interfacial dynamic behaviors in the microchannel with active water pumping.

**Figure 14** Phase change behavior in a 200 μm×300 μm microchannel (Laser power: 40 mW, spot position: 100 μm).

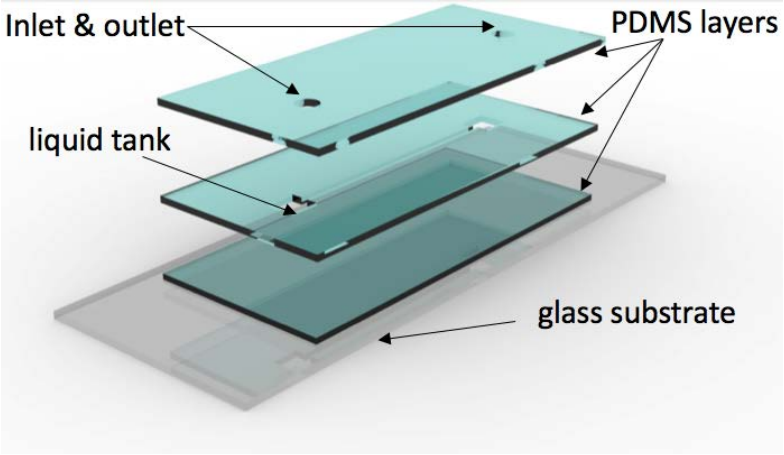

(a)

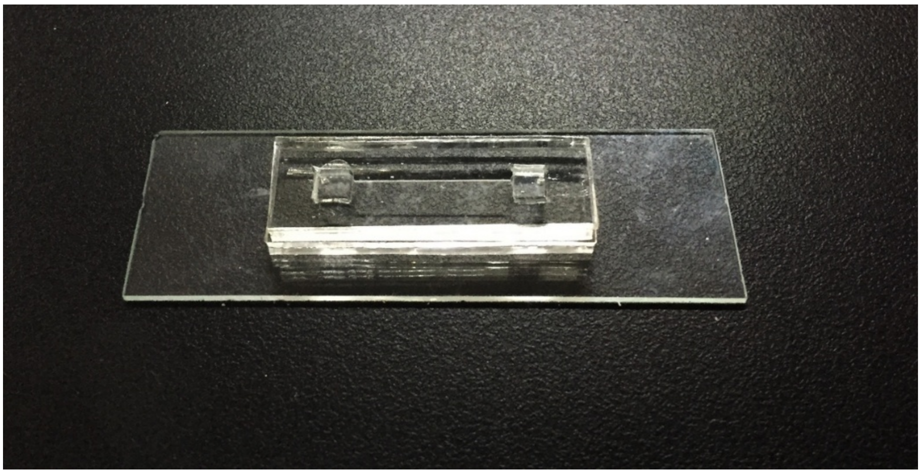

(b)

Fig. 1 (a) Illustration of the microchannel assembly and (b) the image of the fabricated microchannel.

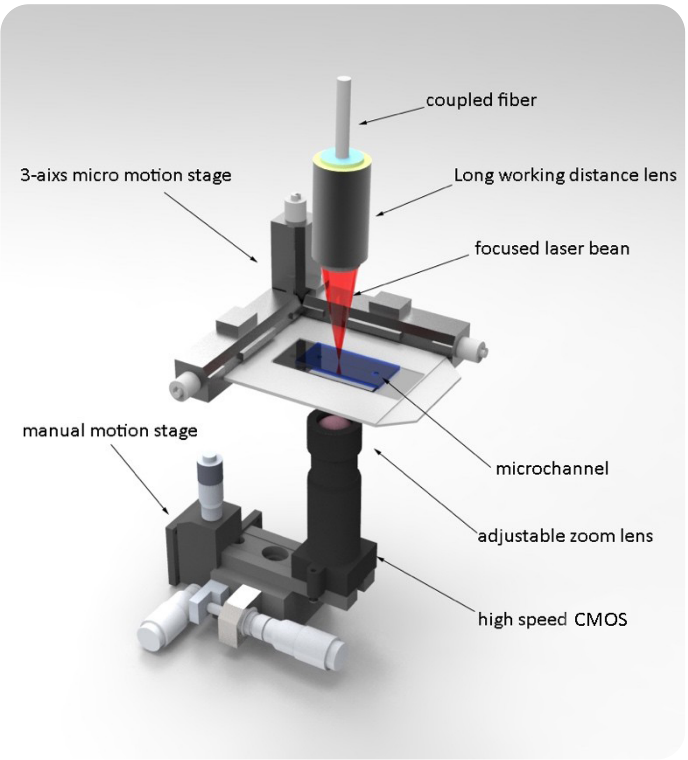

Fig. 2 Schematic diagram of the visualized experimental system.

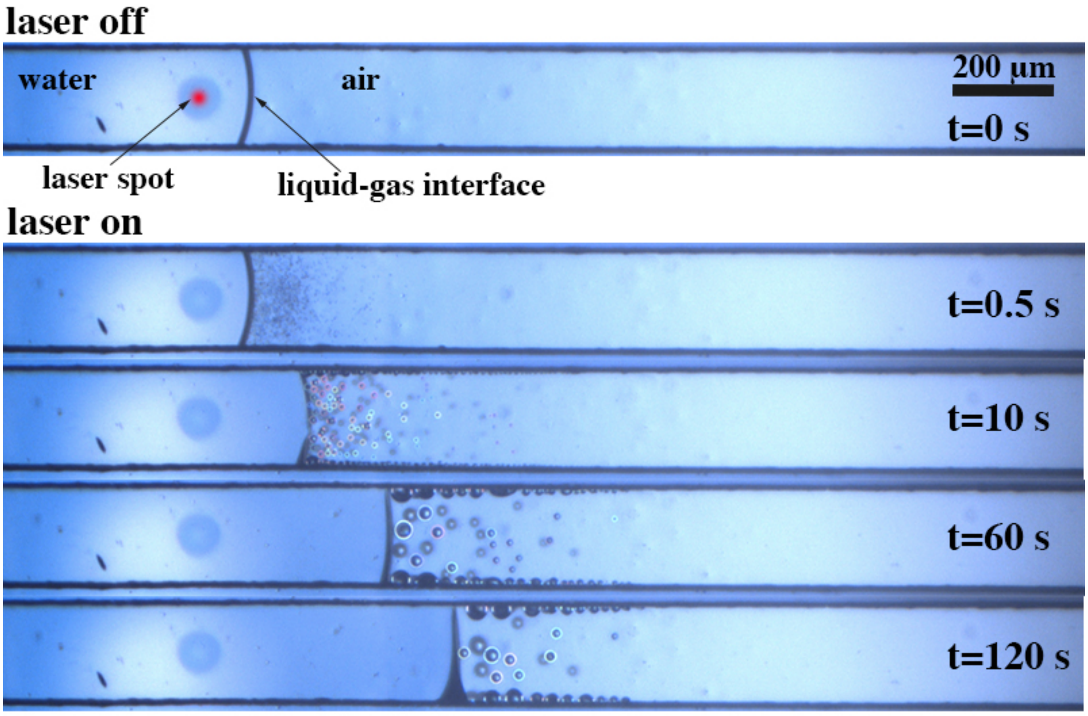

Fig. 3 Phase change behaviors in a 200 μm×100 μm microchannel (Laser power: 10 mW, spot position: 100 μm).

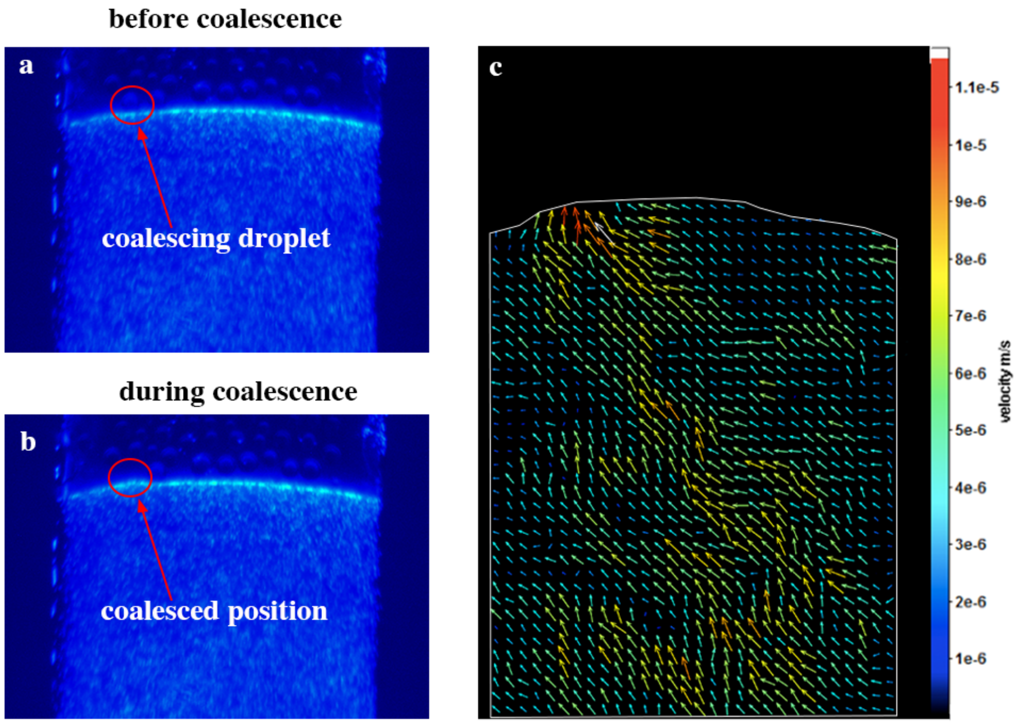

Fig. 4 (a) Raw particle image before coalescence, (b) during coalescence, (c) Velocity vector map of liquid column during the coalescence with single droplet in a 200 μm×100 μm microchannel (Laser power: 10 mW, spot position: 100 μm).

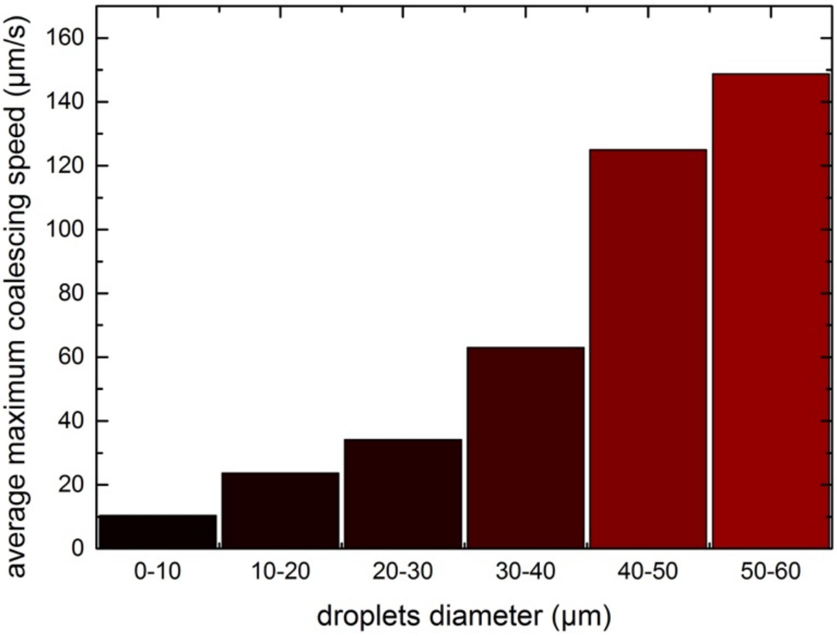

Fig. 5 Effect of the coalesced droplet size on the average maximum coalescing speed in the liquid column (Laser power: 10 mW, spot position: 100 μm).

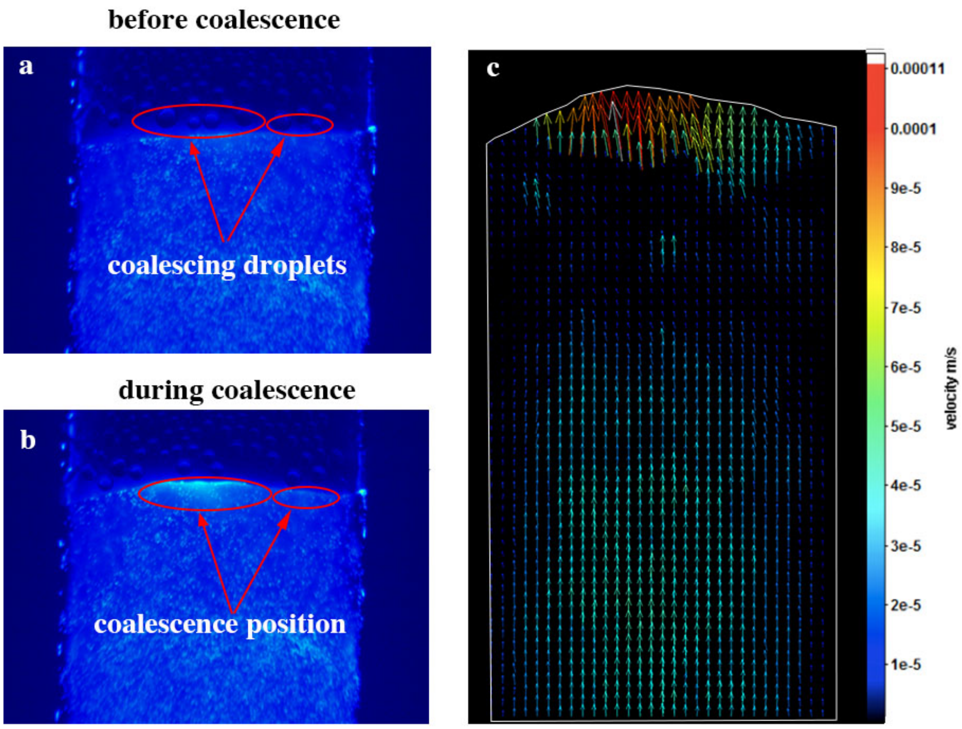

Fig. 6 (a) Raw particle image before coalescence, (b) during coalescence, (c) Velocity vector map of liquid column before and during the coalescence with multiple droplets in a 200 μm×100 μm microchannel (Laser power: 10 mW, spot position: 100 μm).

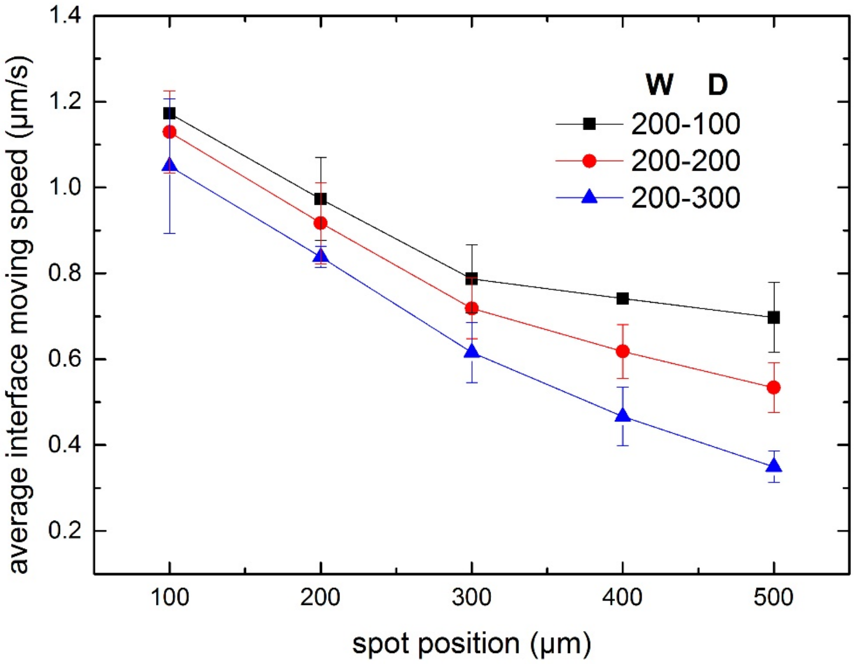

Fig. 7 Effect of the microchannel depth on the average interface moving speed (Laser power: 10 mW).

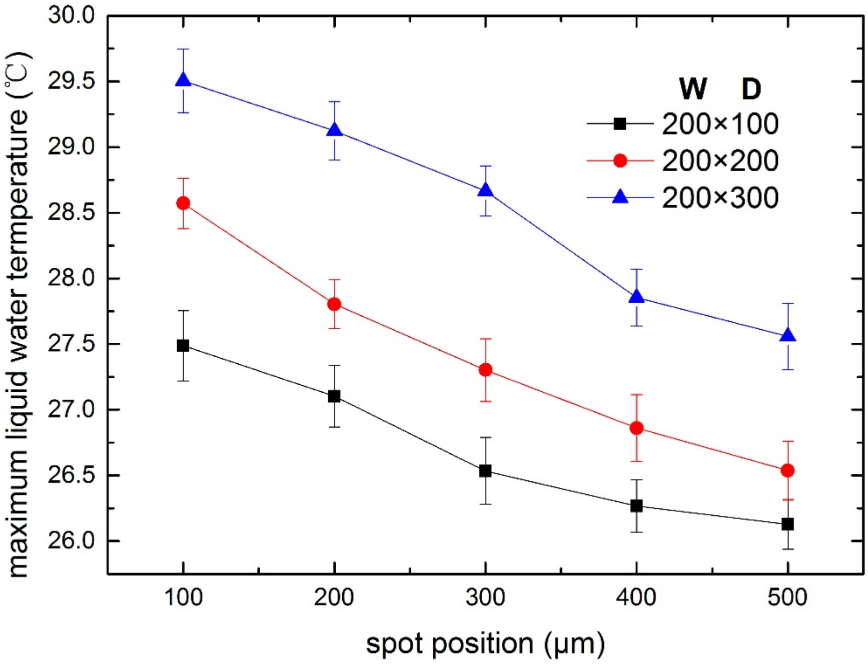

Fig. 8 Variations in the maximum liquid water temperature with the microchannel depth and laser sport position (Laser power: 10 mW).

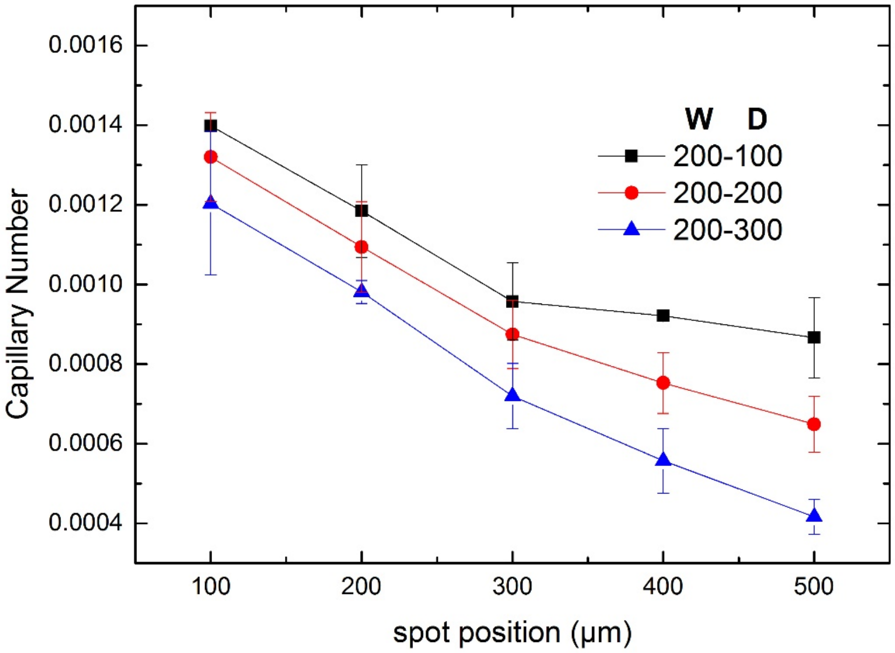

Fig. 9 Variation of Capillary number with the microchannel depth and laser spot position. (Laser power: 10 mW)

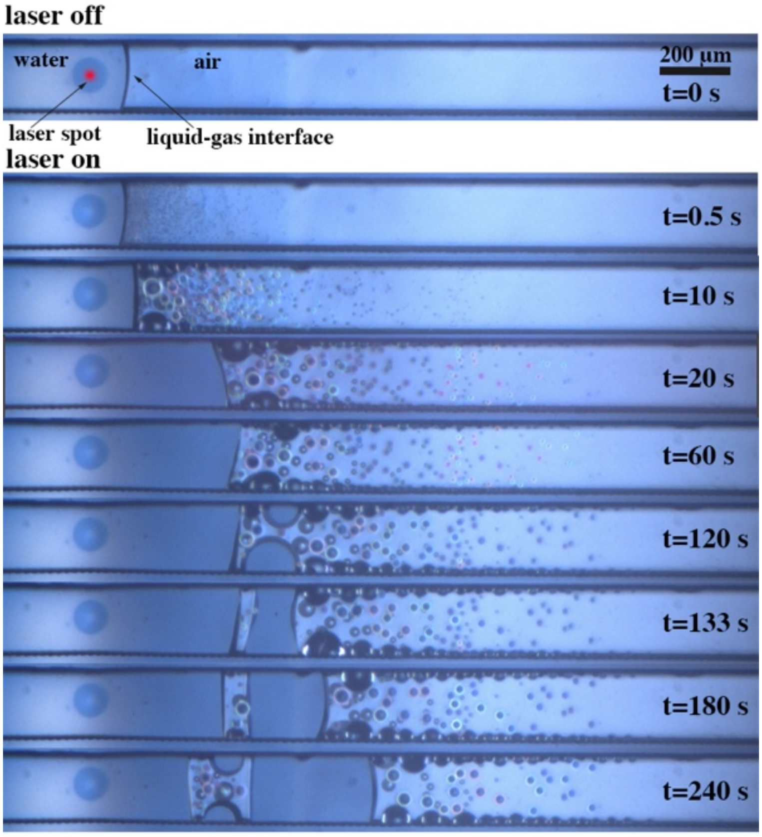

Fig. 10 Phase change behavior in a 200 μm×100 μm microchannel (Laser power: 40 mW, spot position: 100 μm).

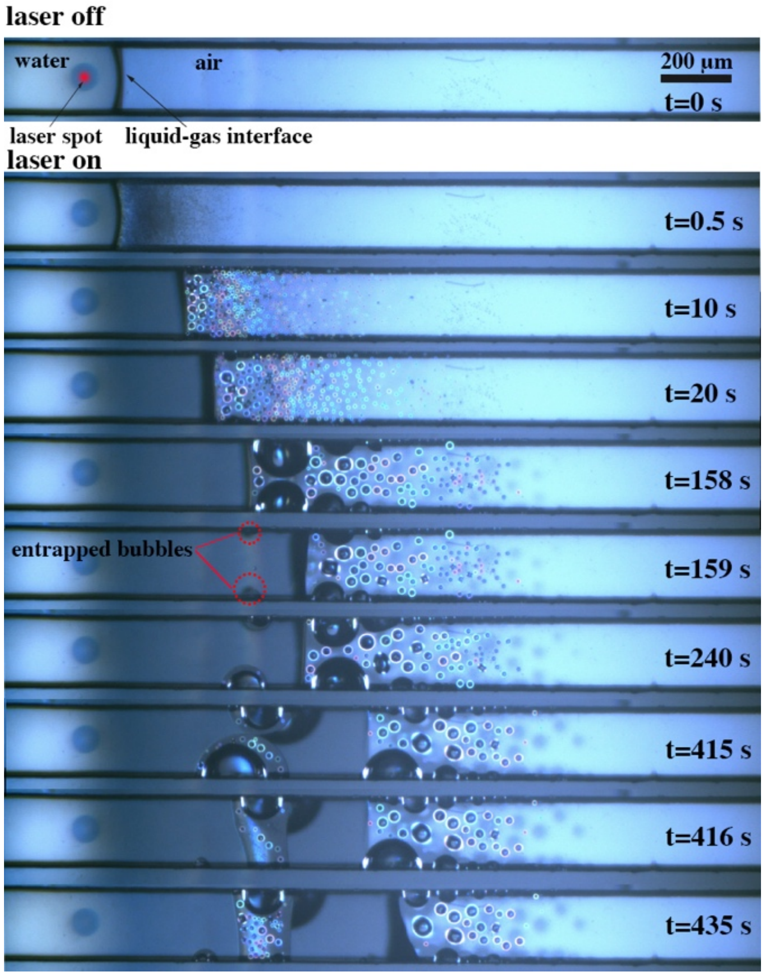

Fig. 11 Phase change behavior in a 200 μm×200 μm microchannel (Laser power: 40 mW, spot position: 100 μm).

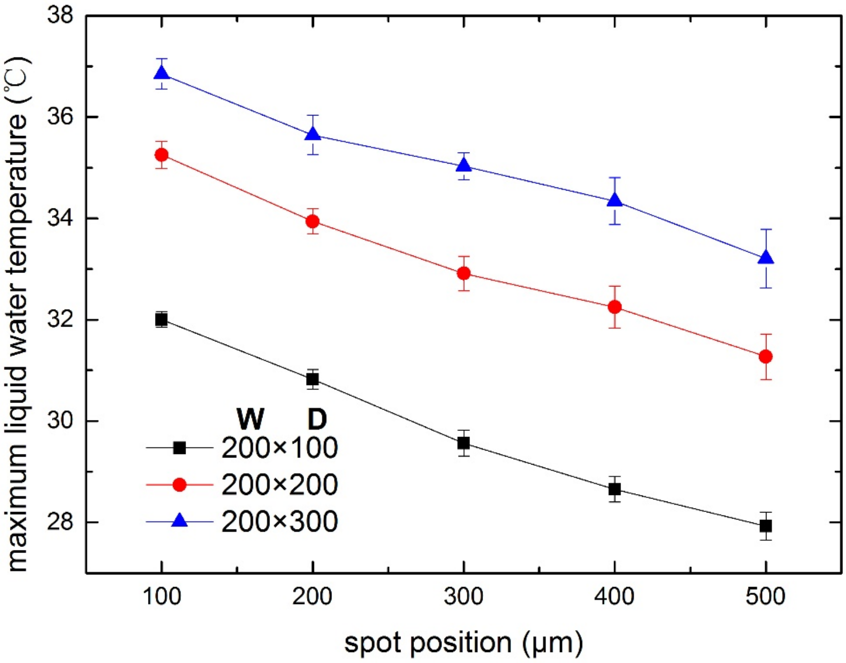

Fig. 12 Variations in the maximum liquid water temperature with the microchannel depth and laser spot position (Laser power: 40 mW).

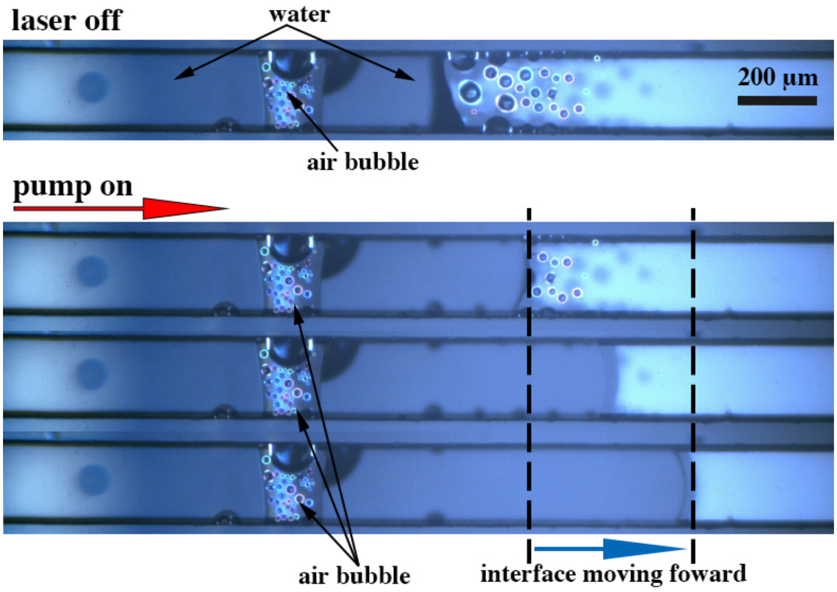

Fig. 13 Interfacial dynamic behaviors in the microchannel with active water pumping.

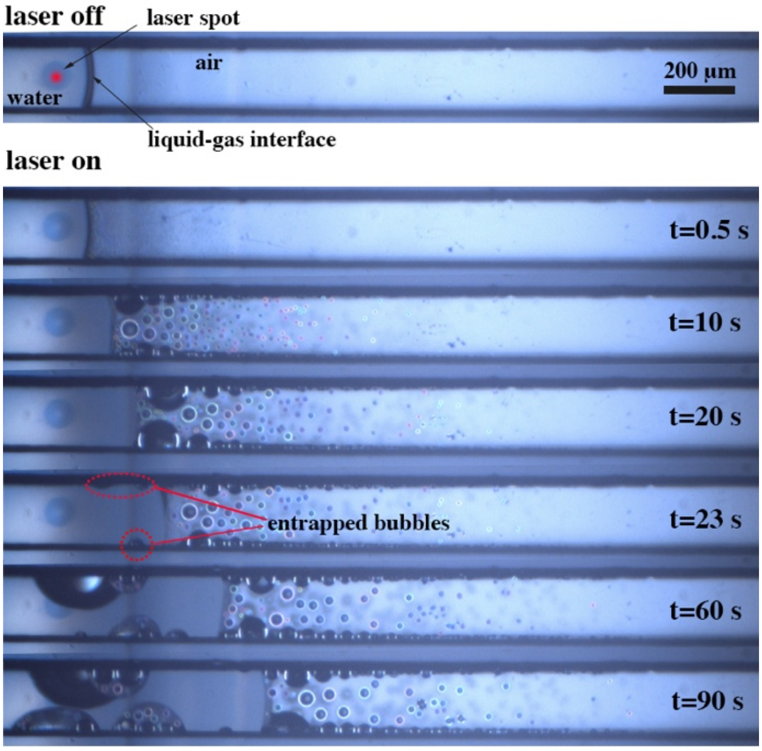

Fig. 14 Phase change behavior in a 200 μm×300 μm microchannel (Laser power: 40 mW, spot position: 100 μm).

# Table of Contents